Available online at www.sciencedirect.com
SCIENCE DIRECT®
Journal of Computational Physics 193 (2004) 642–665
JOURNAL OF COMPUTATIONAL PHYSICS
www.elsevier.com/locate/jcp

Investigation of bend and shear waves in a geometrically exact elastic rod model

T.C. Bishop [a,*], R. Cortez [b,1], O.O. Zhmudsky [c,2]

[a] Center for Bioenvironmental Research at Tulane and Xavier Universities, 1430 Tulane Avenue, SL-3, New Orleans, LA 70112, USA
[b] Department of Mathematics, Tulane University, 6823 St. Charles Avenue, New Orleans, LA 70118, USA
[c] Center for Computational Science, Tulane University, 310 Richardson Building, New Orleans, LA 70118, USA

Received 2 June 2003; received in revised form 5 August 2003; accepted 25 August 2003

Abstract

The propagation of bend and shear waves through an elastic rod is investigated in the framework of geometrically exact nonlinear elasticity. The model allows for shear, extension/compression, bend and twist thus enabling the study of the dynamics of all types of elastic deformations. Numerical and analytical solutions demonstrate that the propagation of planar bend or shear disturbances of finite wavelength require bend, shear and extension/compression waves. For the case of an intrinsically straight, twisted rod an exact large amplitude solution for bend–shear waves is found. In this case, the rod has a helical shape and it rotates in a clockwise or counterclockwise direction. An exact analytical solution for the large amplitude shear oscillation of a straight, untwisted rod is derived. The same type of oscillation for a twisted rod is demonstrated to exist numerically. For the case of an intrinsically straight, untwisted rod, asymptotic theory predicts that the amplitude of the extension/compression wave is proportional to the square of the amplitude of the bend or shear wave and the wavelength of the extension/compression wave is one-half the wavelength of the bend or shear wave. The propagation of planar disturbances along an intrinsically straight, twisted rod is investigated numerically and compared to an all-atom molecular dynamics simulation of DNA. The simulations are in good qualitative agreement and indicate that the chemical structure of DNA supports elastic wave propagation of the type obtained from the rod model.

PACS: 65M06; 92-08; 73C50

Keywords: Elastic rods; Wave propagation; Bend; Shear

* Corresponding author. Tel.: +1-504-988-6203; fax: +1-504-585-6428.
E-mail addresses: bishop@tulane.edu (T.C. Bishop), rcortez@tulane.edu (R. Cortez), ozhmuds@tulane.edu (O.O. Zhmudsky).
[1] Tel.: +1-504-862-3436.
[2] Tel.: +1-504-862-8396; fax: +1-504-862-8392.

0021-9991/$ - see front matter
doi:10.1016/j.jcp.2003.08.028

1. Introduction

Our analysis of the dynamics of elastic rods is based on a Hamiltonian structure of nonlinear elasticity [1]. The model may be regarded as an extension of the classic Kirchhoff–Love model (see [2,3]) that includes shear and extension/compression. In the framework of this model we investigate the numerical and analytical dynamics of bend and shear deformations.

The static and dynamic properties of elastic rods, rings and helices have been studied for many years using variants of the Kirchhoff model. Such an approach has proven successful for numerous applications in structural mechanics, engineering, biochemistry and biology. Some applications include the analysis of loop formation of sub-oceanic cables [4–7], the phenomenon of helix hand reversal in climbing plants [8], and the dynamics of cracking whips [9]. Since the 1970s (see for example [10,11]) elastic rod models have been employed to study the structure of DNA, and more recently, even the dynamics of DNA (see, for example [12,13]).

Closed form expressions for the equilibrium conformations of a Kirchhoff rod [14] and an elastic rod with shear and extension [15] have been obtained by Shi and Hearst and related to the observed folding of DNA into extended and condensed chromatin [16–18]. Goriely and co-workers extended the mathematical analysis by providing a classification of the equilibrium conformations [19] and a theoretical framework for determining their dynamic stability [20].

Previous works on the dynamics of elastic rods have focused on planar motions [21] and traveling waves [22], including the time evolution of planar, twist-free motion of an inextensible and unshearable elastic rod [23]. Many investigations assume the rod is inextensible and/or unshearable. Such restrictions are not necessary, and do not allow for types of motion presented here. Our focus is on the dynamics of elastic rods that excite bend, shear, and extension/compression deformations and that possess an intrinsic shape (straight or twisted).

One of the long-term goals of the study of elastic rod models is to determine to what extent they can be used to simulate the dynamics of long polymer chains, such as DNA, when the number of atoms is too large for an all-atom simulation to be feasible. The elastic rod model addressed here requires the choice of constants that represent physical dimensions of the phenomenon under consideration and elastic properties of the material. The constants used throughout this article are roughly those corresponding to DNA, which are comparable to those of soft materials like polyethylene or rubber. For such materials consideration of all types of motion (bend, shear, twist, and extension) is warranted. We also assume that the length of any excitation is much greater than the atomic length scales characteristic of DNA (i.e. the distance between atoms or base-pairs). Such assumptions are typical in the description of solids, liquids and gases [24,25]. Thus, for our purposes an infinitesimally small volume element means small compared to the wavelength or radius of curvature under consideration, but large compared with the distance between the base-pairs in DNA.

Section 2 presents a description of the system of equations, our choice of elastic constants used throughout the paper and the dimensionless form of the equations used in the computations. In Section 3 we present an exact solution of the equations for the case when the intrinsic shape of the rod is straight and twisted. We show that the propagation of waves along this rod results in nonplanar (helical) motion. We also present the exact solution for a special case of pure shear oscillations. In Section 4 we discuss the case of an intrinsically straight, untwisted rod. The propagation of bend–shear waves through this rod requires the presence of a small amplitude extension/compression wave. This is shown through an approximate solution. Section 5 describes the numerical methods utilized and presents numerical solutions of several examples. We conclude with a comparison of the planar bend–shear motion of an elastic rod to an all-atom molecular dynamics simulation of 158 base-pairs of DNA with similar initial conditions. The purpose of the comparison is to verify that under similar conditions, the elastic rod model yields results that agree well with simulations based on traditional molecular mechanics.

2. System of equations for elastic rod dynamics

Our model is based on a system of equations describing a geometrically exact model of an elastic rod [1]. As seen in the laboratory frame, the centerline of the rod is represented by $\vec{r}(s,t) \in \mathbb{R}^3$, where s is the fiducial arclength [26] and t is time. Fiducial arclength is the arclength parameter of the uncompressed or unstretched rod; however, during dynamics, the rod's arclength may not coincide with fiducial arclength. At each point on the rod, its cross-section is conceived as a disk that lies in a plane but not necessarily perpendicular to the centerline tangent vector. In order to describe its orientation, an internal coordinate system, $\{\vec{d}_1, \vec{d}_2, \vec{d}_3\}$, is attached to each cross-section. In this internal coordinate system, $\vec{d}_3$ is perpendicular to the cross-section which is spanned by vectors $\vec{d}_1$ and $\vec{d}_2$. The relative orientation of each vector in adjacent cross-sections describes the local bend and twist in the rod. The rod centerline $\vec{r}(s,t)$ and the directors $\{\vec{d}_1, \vec{d}_2, \vec{d}_3\}$ are represented in the (global) laboratory frame.

The equations of motion of the rod involve four vector functions $\vec{\Omega}$, $\vec{\Gamma}$, $\vec{\omega}$ and $\vec{\gamma}$ that describe the conformation and dynamics of the rod. These functions are represented in the internal coordinate system, so that $\vec{\Omega} = (\Omega_1, \Omega_2, \Omega_3)$ means $\vec{\Omega} = \Omega_1\vec{d}_1 + \Omega_2\vec{d}_2 + \Omega_3\vec{d}_3$.

The vector $\vec{\Gamma}$ describes the relative translation of the centers of the cross-sections while $\vec{\gamma}$ describes the centerline translational velocity

$$\vec{\gamma} = \frac{\partial \vec{r}}{\partial t}, \quad \vec{\Gamma} = \frac{\partial \vec{r}}{\partial s}. \tag{1}$$

Notice that $\vec{\Gamma}$ is tangent to the rod centerline. Since its three components $\vec{\Gamma} = (\Gamma_1, \Gamma_2, \Gamma_3)$ are given in the internal coordinate system, this implies that whenever $\Gamma_1 = \Gamma_2 = 0$, then $\vec{\Gamma} = \Gamma_3\vec{d}_3$ and therefore $\vec{d}_3$ must align with the centerline tangent vector. In this way, Γ_3 is related to the extension (compression) of the rod, while the components Γ_1 and Γ_2 are related to the shear in the rod (the parallel translation of contiguous cross-sections).

The vector $\vec{\Omega}$ describes the relative rotation of the cross-sections at a fixed time t, while $\vec{\omega}$ is the angular velocity of the cross-section at a fixed position s

$$\frac{\partial \vec{d}_k}{\partial t} = \vec{\omega} \times \vec{d}_k, \quad \frac{\partial \vec{d}_k}{\partial s} = \vec{\Omega} \times \vec{d}_k. \tag{2}$$

The directors must remain of unit length so any change in space or time must be orthogonal to the corresponding local axis of rotation; Eq. (2) preserve director length. Notice that $\Omega_3 = \vec{\Omega} \cdot \vec{d}_3$ represents the twist in the rod. If $\Omega_1 = \Omega_2 = 0$, then the cross-sections are all parallel to each other. If Ω_1 or Ω_2 is nonzero the cross-sectional planes are not parallel and the rod is bent. In biological terminology the components of $\vec{\Gamma}$ and $\vec{\Omega}$ are the six DNA helical parameters [27] describing translation $\vec{\Gamma} = (\text{shift}, \text{slide}, \text{rise})$ and rotation $\vec{\Omega} = (\text{tilt}, \text{roll}, \text{twist})$.

At times it will be necessary to transform a vector from internal coordinates to laboratory coordinates using the change of basis matrix

$$\hat{T} = \begin{pmatrix} d_{1,X} & d_{2,X} & d_{3,X} \\ d_{1,Y} & d_{2,Y} & d_{3,Y} \\ d_{1,Z} & d_{2,Z} & d_{3,Z} \end{pmatrix}.$$

For example, in order to use the second equation in (1) componentwise, we solve

$$(\hat{T}\vec{\Gamma})_k = \frac{\partial r_k}{\partial s} \quad \text{for } k = 1, 2, 3.$$

The ground state of the rod, or intrinsic shape, is specified by the vectors $\vec{\Gamma}_0$ and $\vec{\Omega}_0$. They represent the conformation of the rod with zero potential energy. In general, these vectors depend on s and t and allow the

rod to have an intrinsic shear and extension, $\vec{\Gamma}_0$, or intrinsic bend and twist, $\vec{\Omega}_0$. The simplest case is a rod with no intrinsic bend or twist, $\vec{\Omega}_0 = (0,0,0)$, and no intrinsic shear but with unit extension, $\vec{\Gamma}_0 = (0,0,1)$.

A geometrically exact model of an elastic rod with all variables corresponding to an internal coordinate representation [1] and with linear constitutive relations [26] is as follows:

$$\rho\left(\frac{\partial\vec{\gamma}}{\partial t} + \vec{\omega}\times\vec{\gamma}\right) = \hat{C}\cdot\frac{\partial(\vec{\Gamma}-\vec{\Gamma}_0)}{\partial s} + \vec{\Omega}\times\left(\hat{C}\cdot\left(\vec{\Gamma}-\vec{\Gamma}_0\right)\right), \tag{3}$$

$$\hat{I}\cdot\frac{\partial\vec{\omega}}{\partial t} + \vec{\omega}\times\left(\hat{I}\cdot\vec{\omega}\right) = \hat{D}\cdot\frac{\partial(\vec{\Omega}-\vec{\Omega}_0)}{\partial s} + \vec{\Omega}\times\left(\hat{D}\cdot\left(\vec{\Omega}-\vec{\Omega}_0\right)\right) + \vec{\Gamma}\times\left(\hat{C}\cdot\left(\vec{\Gamma}-\vec{\Gamma}_0\right)\right), \tag{4}$$

$$\frac{\partial\vec{\Gamma}}{\partial t} + \vec{\omega}\times\vec{\Gamma} = \frac{\partial\vec{\gamma}}{\partial s} + \vec{\Omega}\times\vec{\gamma}, \tag{5}$$

$$\frac{\partial\vec{\Omega}}{\partial t} + \vec{\omega}\times\vec{\Omega} = \frac{\partial\vec{\omega}}{\partial s}. \tag{6}$$

In this system, Eq. (3) represents the balance of force while Eq. (4) represents the balance of torque in internal coordinates. Eqs. (5) and (6) are simply continuity relations expressed in the same frame.

The dynamics are computed in two phases. Eqs. (3)–(6) are solved first for the internal variables; then, Eqs. (1) and (2) are solved to obtain the directors $\{\vec{d}_1,\vec{d}_2,\vec{d}_3\}$ and the centerline $\vec{r}$. These vectors are also necessary for visualization of results.

We will restrict our analysis to diagonal matrices $\hat{I}$, $\hat{C}$ and $\hat{D}$. Matrix $\hat{I}$ is the linear density of the moment of inertia tensor. Matrices $\hat{C}$ and $\hat{D}$ represent the elastic properties of the rod according to Hooke's Law (C_3 is the stretch modulus, C_1 and C_2 are shear moduli, D_3 is the torsional rigidity, D_1 and D_2 are bend stiffnesses). In the remainder of this paper we consider only isotropic shear $C_1 = C_2 = C$ and isotropic bend $D_1 = D_2 = D$. The linear mass density of the rod is ρ.

2.1. Choice of constants

For a homogeneous body of given Young, Y, and shear, μ, moduli the torsion rigidity and bend stiffness are related to the geometry of the object. For circular cross-sections of radius R, $D_3 = \frac{1}{2}\mu\pi R^4$ and $D = \frac{1}{4}Y\pi R^4$ [41]. For DNA, the elastic properties are often determined in such a way that one of the elastic constants is measured and another is calculated based on some additional assumption. For example, the ratio of the torsional rigidity to bending stiffness, denoted ε and equivalent to $2\mu/Y$, is often reported along with Y. Many experiments and theoretical estimates place ε in the interval $0.7 \leqslant \varepsilon \leqslant 1.7$ (see [42–46]). In this study we use the representative value of 1087 pN for the stretch modulus of DNA [36], corresponding to a Young modulus of 3.46×10^8 Pa, and a ratio $D_3 = 1.67D$.

In this case the elastic constants have the values $I = 8.05\times10^{-34}[KM]$, $C = 9.08\times10^{-10}[KM/S^2]$, and $D = 2.75\times10^{-28}[KM^3/S^2]$. We will also use the value $\rho = 3.22\times10^{-15}[K/M]$. This results in the matrices

$$\hat{I} = 8.05\times10^{-34}\begin{pmatrix}1&0&0\\0&1&0\\0&0&2\end{pmatrix}[KM], \tag{7}$$

$$\hat{C} = 9.08\times10^{-10}\begin{pmatrix}1&0&0\\0&1&0\\0&0&1.19\end{pmatrix}\left[\frac{KM}{S^2}\right], \tag{8}$$

$$\hat{D} = 2.75 \times 10^{-28} \begin{pmatrix} 1 & 0 & 0 \\ 0 & 1 & 0 \\ 0 & 0 & 1.67 \end{pmatrix} \left[\frac{KM^3}{S^2} \right]. \tag{9}$$

Thus the elastic properties of DNA are similar to that of polyethylene ($2–7 \times 10^8$ Pa) or rubber ($1–10 \times 10^7$ Pa). By comparison an iron (Young's modulus of 2.0×10^{11} Pa) nanowire (radius 1 nm) will have a stretch modulus of 628 000 pN, approximately 600 times greater than that of DNA.

2.2. Dimensionless form of the equations

For the numerical analysis of Eqs. (3)–(6) it is convenient to introduce time and length scales (τ and ℓ). Then relations between dimensional and dimensionless variables (denoted by an asterisk) will be:

$$\begin{aligned} &t = \tau t^*, \quad s = \ell s^*, \quad \omega = \frac{1}{\tau}\omega^*, \\ &\Omega = \frac{1}{\ell}\Omega^*, \quad \gamma = \frac{\ell}{\tau}\gamma^*, \quad \Gamma = \Gamma^*. \end{aligned} \tag{10}$$

Substitution of expressions (10) into (3)–(6) yields:

$$\frac{\partial \vec{\gamma}^*}{\partial t^*} + \vec{\omega}^* \times \vec{\gamma}^* = \hat{C}^* \cdot \frac{\partial(\vec{\Gamma}^* - \vec{\Gamma}_0^*)}{\partial s^*} + \vec{\Omega}^* \times \left(\hat{C}^* \cdot \left(\vec{\Gamma}^* - \vec{\Gamma}_0^* \right) \right), \tag{11}$$

$$\hat{I}^* \cdot \frac{\partial \vec{\omega}^*}{\partial t^*} + \vec{\omega}^* \times \left(\hat{I}^* \cdot \vec{\omega}^* \right) = \hat{D}^* \cdot \frac{\partial(\vec{\Omega}^* - \vec{\Omega}_0^*)}{\partial s^*} + \vec{\Omega}^* \times \left(\hat{D}^* \cdot \left(\vec{\Omega}^* - \vec{\Omega}_0^* \right) \right) + \vec{\Gamma}^* \times \left(\hat{C}^* \cdot \left(\vec{\Gamma}^* - \vec{\Gamma}_0^* \right) \right), \tag{12}$$

$$\frac{\partial \vec{\Gamma}^*}{\partial t^*} + \vec{\omega}^* \times \vec{\Gamma}^* = \frac{\partial \vec{\gamma}^*}{\partial s^*} + \vec{\Omega}^* \times \vec{\gamma}^*, \tag{13}$$

$$\frac{\partial \vec{\Omega}^*}{\partial t^*} + \vec{\omega}^* \times \vec{\Omega}^* = \frac{\partial \vec{\omega}^*}{\partial s^*}, \tag{14}$$

where

$$\hat{C}^* = \frac{\hat{C}}{\rho}\left(\frac{\tau}{\ell}\right)^2, \quad \hat{D}^* = \frac{\hat{D}}{I}\left(\frac{\tau}{\ell}\right)^2, \quad \hat{I}^* = \frac{\hat{I}}{I}. \tag{15}$$

A simple choice for these scales is $\tau = \sqrt{I/C} = 9.4 \times 10^{-13}[S]$ and $\ell = \sqrt{I/\rho} = 5.0 \times 10^{-10}[M]$. This yields $\hat{C}^* = \hat{C}/C$ and $\hat{D}^* = \frac{D\rho}{IC}(\hat{D}/D)$, where $D\rho/IC = 1.21$ is equivalent to the square of the ratio of bend to shear velocities. From this point on, the asterisk will be omitted.

From (15) we can see that Eqs. (11)–(14) depend only on the ratio τ/ℓ. Thus, for example, the simulation results obtained for the rod length 0.5 nm and final time 0.94 ps will be the same as for the length 50 nm and final time 94 ps.

3. Bend and shear waves: exact analytical solutions

3.1. Intrinsically straight, twisted rod

In this section we consider an intrinsically straight, twisted rod with $\vec{\Gamma}_0 = (0, 0, \Gamma_{03})$ and $\vec{\Omega}_0 = (0, 0, \Omega_{03})$. In this case we can separate the variables into transverse variables $\vec{\gamma}_\perp \equiv (\gamma_1, \gamma_2, 0)$, $\vec{\Gamma}_\perp \equiv (\Gamma_1, \Gamma_2, 0)$, $\vec{\omega}_\perp \equiv (\omega_1, \omega_2, 0)$, $\vec{\Omega}_\perp \equiv (\Omega_1, \Omega_2, 0)$ and longitudinal variables γ_3, $\Gamma_3 = \Gamma_{03} + \delta\Gamma_3$, ω_3, $\Omega_3 = \Omega_0 + \delta\Omega_3$. We obtain an exact solution of the fully nonlinear system in which the longitudinal variables do not appear: $\gamma_3 = \omega_3 = \delta\Gamma_3 = \delta\Omega_3 = 0$. With this restriction, the nonlinear system (11)–(14) reduces to:

$$\frac{\partial \vec{\gamma}_\perp}{\partial t} = \frac{\partial \vec{\Gamma}_\perp}{\partial s} + \left[\vec{\Omega}_0 \times \vec{\Gamma}_\perp\right], \tag{16}$$

$$\frac{\partial \vec{\omega}_\perp}{\partial t} = D_1 \frac{\partial \vec{\Omega}_\perp}{\partial s} + D_1\left[\vec{\Omega}_0 \times \vec{\Omega}_\perp\right] + \left[\vec{\Gamma}_0 \times \vec{\Gamma}_\perp\right], \tag{17}$$

$$\frac{\partial \vec{\Gamma}_\perp}{\partial t} = \frac{\partial \vec{\gamma}_\perp}{\partial s} + \left[\vec{\Gamma}_0 \times \vec{\omega}_\perp\right] + \left[\vec{\Omega}_0 \times \vec{\gamma}_\perp\right], \tag{18}$$

$$\frac{\partial \vec{\Omega}_\perp}{\partial t} = \frac{\partial \vec{\omega}_\perp}{\partial s} + \left[\vec{\Omega}_0 \times \vec{\omega}_\perp\right] \tag{19}$$

plus the three algebraic constraints:

$$\vec{\omega}_\perp \times \vec{\gamma}_\perp = \vec{\Omega}_\perp \times \vec{\Gamma}_\perp, \tag{20}$$

$$\vec{\omega}_\perp \times \vec{\Gamma}_\perp = \vec{\Omega}_\perp \times \vec{\gamma}_\perp, \tag{21}$$

$$\vec{\omega}_\perp \times \vec{\Omega}_\perp = 0. \tag{22}$$

We may look for a solution of the form

$$\begin{aligned}
&\Gamma_1 = \Gamma_1^A \cos(\omega t - ks), \quad \Gamma_2 = \Gamma_2^A \sin(\omega t - ks),\\
&\gamma_1 = \gamma_1^A \cos(\omega t - ks), \quad \gamma_2 = \gamma_2^A \sin(\omega t - ks),\\
&\omega_1 = \omega_1^A \cos(\omega t - ks), \quad \omega_2 = \omega_2^A \sin(\omega t - ks),\\
&\Omega_1 = \Omega_1^A \cos(\omega t - ks), \quad \Omega_2 = \Omega_2^A \sin(\omega t - ks)
\end{aligned}$$

leading to a system of equations for the wave amplitudes given by

$$\begin{aligned}
&\omega\gamma_{1,2}^A = -k\Gamma_{1,2}^A + \Omega_{03}\Gamma_{2,1}^A,\\
&\omega\omega_{1,2}^A = -kD_1\Omega_{1,2}^A + D_1\Omega_{03}\Omega_{2,1}^A + \Gamma_{03}\Gamma_{2,1}^A,\\
&\omega\Gamma_{1,2}^A = -k\gamma_{1,2}^A + \Gamma_{03}\omega_{2,1}^A + \Omega_{03}\gamma_{2,1}^A,\\
&\omega\Omega_{1,2}^A = -k\omega_{1,2}^A + \Omega_{03}\omega_{2,1}^A.
\end{aligned}$$

Since the equations with the second subscript are exactly the same as the equations with the first subscript, we conclude that the solution will satisfy

$$\begin{pmatrix} \gamma_2^A \\ \omega_2^A \\ \Gamma_2^A \\ \Omega_2^A \end{pmatrix} = \pm \begin{pmatrix} \gamma_1^A \\ \omega_1^A \\ \Gamma_1^A \\ \Omega_1^A \end{pmatrix}$$

and use this to solve the smaller system

$$\begin{pmatrix} \omega & 0 & (k \pm \Omega_{03}) & 0 \\ 0 & \omega & \pm\Gamma_{03} & D_1(k \pm \Omega_{03}) \\ (k \pm \Omega_{03}) & \pm\Gamma_{03} & \omega & 0 \\ 0 & (k \pm \Omega_{03}) & 0 & \omega \end{pmatrix} \begin{pmatrix} \gamma_1^A \\ \omega_1^A \\ \Gamma_1^A \\ \Omega_1^A \end{pmatrix} = 0, \tag{23}$$

where we have defined $\kappa_{\mathrm{p,m}} = (k \pm \Omega_{03})$.

A nontrivial solution of the system (16)–(19) takes the form

$$\begin{aligned} \Gamma_1 &= \Gamma_1^A \cos(\omega t - ks), \\ \Gamma_2 &= \mp\Gamma_1^A \sin(\omega t - ks), \\ \omega_1 &= \mp\frac{\omega\Gamma_{03}}{\omega^2 - D_1\kappa_{\mathrm{p,m}}^2}\Gamma_1^A \cos(\omega t - ks), \\ \omega_2 &= \frac{\omega\Gamma_{03}}{\omega^2 - D_1\kappa_{\mathrm{p,m}}^2}\Gamma_1^A \sin(\omega t - ks), \\ \gamma_1 &= -\frac{\kappa_{\mathrm{p,m}}}{\omega}\Gamma_1^A \cos(\omega t - ks), \\ \gamma_2 &= \pm\frac{\kappa_{\mathrm{p,m}}}{\omega}\Gamma_1^A \sin(\omega t - ks), \\ \Omega_1 &= \pm\frac{\kappa_{\mathrm{p,m}}\Gamma_{03}}{\omega^2 - D_1\kappa_{\mathrm{p,m}}^2}\Gamma_1^A \cos(\omega t - ks), \\ \Omega_2 &= -\frac{\kappa_{\mathrm{p,m}}\Gamma_{03}}{\omega^2 - D_1\kappa_{\mathrm{p,m}}^2}\Gamma_1^A \sin(\omega t - ks), \end{aligned} \tag{24}$$

where it is clear that the coefficients depend on the frequency, wave number, intrinsic shape and elastic constants. Although there are no more degrees of freedom, it turns out that the algebraic constraints (20)–(22) are identically satisfied provided the frequency ω solves the dispersion relation

$$\left(\omega^2 - \kappa_{\mathrm{p,m}}^2 D_1\right)\left(\omega^2 - \kappa_{\mathrm{p,m}}^2\right) = \omega^2\Gamma_{03}^2. \tag{25}$$

Here $\kappa_{\mathrm{p,m}}$ are "modified" wave numbers $\kappa_{\mathrm{p}} = k + \Omega_{03}$ and $\kappa_{\mathrm{m}} = k - \Omega_{03}$ which take into account the intrinsic twist and its handedness. For this discussion we assume that $\Omega_{03} \geqslant 0$ although this is not a restriction. It is worth pointing out that since there has been no linearization of the system of equations, the solution in Eq. (24) is exact for any value of the amplitude Γ_1^A.

The last equation gives four possible frequencies:

$$\omega_{\pm}^{\mathrm{p,m}} = \frac{1}{2}\left\{\sqrt{\kappa_{\mathrm{p,m}}^2\left(\sqrt{D_1}+1\right)^2 + \Gamma_{03}^2} \pm \sqrt{\kappa_{\mathrm{p,m}}^2\left(\sqrt{D_1}-1\right)^2 + \Gamma_{03}^2}\right\}, \tag{26}$$

since for each choice of sign there are also two choices of modified wave numbers κ_{p} and κ_{m}. The four branches of dispersion in an intrinsically twisted rod are graphed in Fig. 1. We note that when $\Omega_{03} = 0$ the modified wave numbers satisfy $\kappa_{\mathrm{m}} = \kappa_{\mathrm{p}} = k$ and so the four branches reduce to only two branches. This

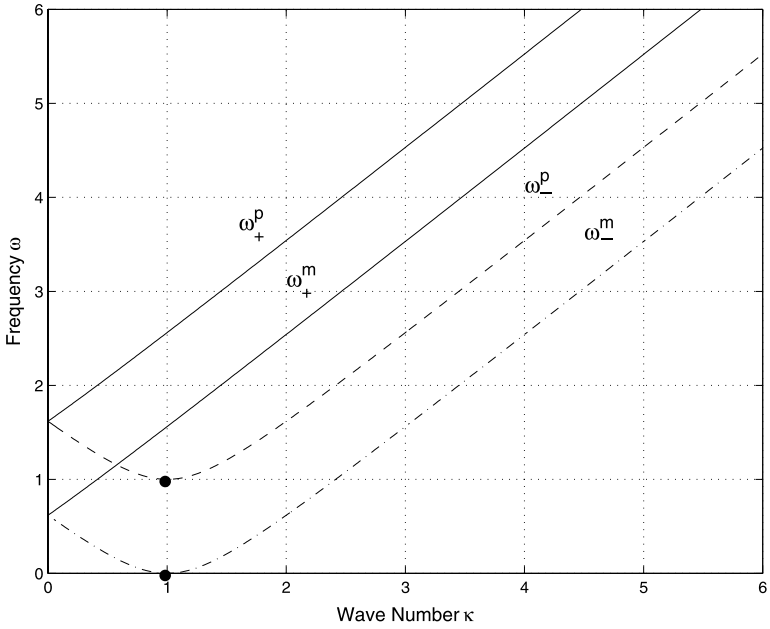

Fig. 1. Dispersion of large amplitude bend–shear waves in an intrinsically-twisted rod. The intrinsic twist was set to $\Omega_{03} = 1$.

case will be discussed in the next section. The wave type, predominantly bend or predominantly shear, depends on the frequency and the wave number.

For the case $k \approx \Omega_{03}$ (i.e. $\kappa_m \to 0$), we have the parabolic relations $\omega_-^m \approx \kappa_m^2\sqrt{D_1}/\Gamma_{03}$ and $\omega_+^m \approx \Gamma_{03} + \kappa_m^2(D_1+1)/2\Gamma_{03}$. These cases are indicated by the two solid dots in Fig. 1.

The association of the limiting behavior of $\omega_\pm^{p,m}$ with different wave types can also be verified by using expressions (24) to compute the ratio of shear energy to bend energy (see Appendix A)

$$\frac{\Gamma_\perp^2}{D_1\Omega_\perp^2} = \frac{\left[(\omega_\pm^{p,m})^2 - \kappa_{p,m}^2 D_1\right]^2}{D_1\kappa_{p,m}^2\Gamma_{03}^2}. \tag{27}$$

Fig. 2 shows this ratio for all four branches and a range of wave numbers. When this ratio is large, the waves are dominated by shear and when the ratio is small, the waves are dominated by bend. We point out that when k tends to Ω_{03}, the energy ratio tends to zero in the case of ω_-^m (indicating predominantly bend motion) and to infinity for ω_+^m (indicating predominantly shear motion).

For $\Omega_{03} \neq 0$, the short wavelength limit, $k \to \infty$, yields $\omega_+^{p,m} \approx \kappa_{p,m}\sqrt{D_1}$ and corresponds to bend waves. Similarly, $\omega_-^{p,m} \approx \kappa_{p,m}$ and therefore corresponds to shear waves. In the long wavelength limit, $k \to 0$, the solution is generally a combination of shear and bend waves.

Although, in general, the solution in Eq. (24) is a combination of bend and shear waves, it is interesting to see what happens to this solution in the limit $\kappa_m \to 0$. The parabolic profile in Fig. 1 corresponding to ω_+^m is characterized by $\omega \to \Gamma_{03}$ and $k \to \Omega_{03}$ so that the solution becomes

$$\begin{aligned}
\vec{\omega}(s,t) &= \Gamma_1^A(\cos(\Gamma_{03}t - \Omega_{03}s), \sin(\Gamma_{03}t - \Omega_{03}s), 0),\\
\vec{\Gamma}(s,t) &= (\Gamma_1^A\cos(\Gamma_{03}t - \Omega_{03}s), \Gamma_1^A\sin(\Gamma_{03}t - \Omega_{03}s), \Gamma_{03}),\\
\vec{\gamma}(s,t) &= (0,0,0),\\
\vec{\Omega}(s,t) &= (0,0,\Omega_{03}),
\end{aligned}$$

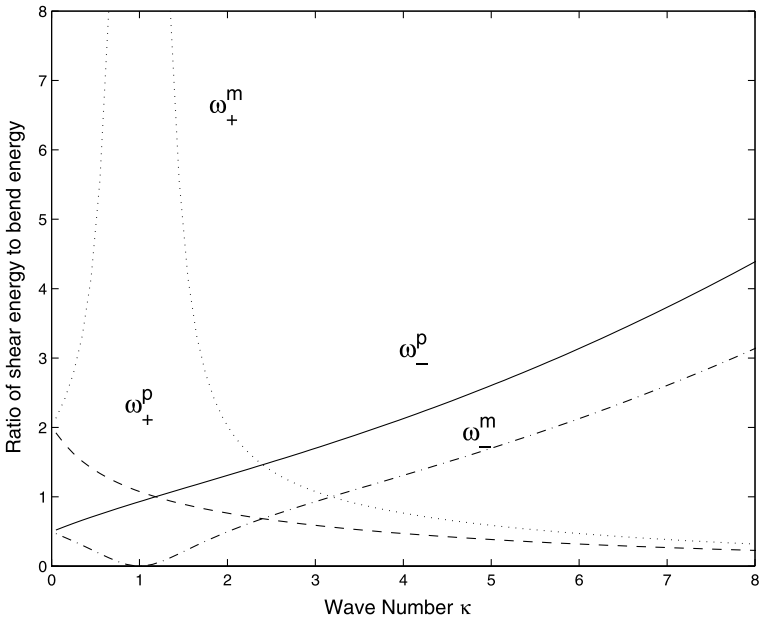

Fig. 2. Ratio of shear/bend energies for $\omega_{+}^{\mathrm{p,m}}$ and $\omega_{-}^{\mathrm{p,m}}$. The intrinsic twist was set to $\Omega_{03} = 1$.

which is an extension-free pure shear solution. This is consistent with the corresponding curve in Fig. 2 where the shear-to-bend ratio increases without bound. On the other hand, the parabolic profile in Fig. 1 corresponding to ω_{-}^{m} is characterized by $\omega_{-}^{\mathrm{m}} \approx \kappa_{\mathrm{m}}^2 \sqrt{D_1}/\Gamma_{03}$ and $k \to \Omega_{03}$. We find this limit by holding the amplitude of the bend waves fixed to get the time-independent pure bend solution

$$\begin{aligned}
&\vec{\omega}(s,t) = (0,0,0),\\
&\vec{\Gamma}(s,t) = (0,0,\Gamma_{03}),\\
&\vec{\gamma}(s,t) = \Omega^A \sqrt{D_1}(\cos(\Omega_{03}s), -\sin(\Omega_{03}s), 0),\\
&\vec{\Omega}(s,t) = (-\Omega^A \cos(\Omega_{03}s), \Omega^A \sin(\Omega_{03}s), \Omega_{03}).
\end{aligned}$$

This is consistent with the corresponding curve in Fig. 2 where the shear-to-bend ratio is zero for $k = \Omega_{03}$. It turns out that these solutions are translating twisted rings.

To visualize the dynamics, a numerical solution of the nonlinear system of Eqs. (11)–(14) was computed using Eq. (24) as initial conditions, with shear amplitude $\Gamma_1^A = 0.5$, $k = 2$, $\Omega_{03} = 1$, $\Gamma_{03} = 1$ and ω_{+}^{p}. Fig. 3 shows five snapshots representing one period ($t = 1.25$) of this bend–shear wave.

By simple inspection of Eq. (24) one can see that $\vec{\omega}$ is a scalar multiple of $\vec{\Omega}$, and thus one can verify that $\vec{d}_k(s,t)$ has the form of a traveling wave with speed $\omega/\kappa_{\mathrm{p,m}}$. With this in mind, one can also deduce that the centerline $\vec{r}(s,t)$ is a superposition of traveling waves. This is supported by the numerical solution, which indicates that the main motion of the rod is that of a rotating helix. We point out that due to the form of $\vec{d}_k(s,t)$, the rotation of the helix is affected by the intrinsic twist. In the case of $\kappa_{\mathrm{m}} = k - \Omega_{03}$, the rotation may change direction depending on the sign of κ_{m} (see Fig. 1).

3.1.1. Pure shear oscillation of a twisted rod

A twisted rod admits a particular but interesting type of pure shear oscillation. To obtain this solution we first consider a straight rod with no intrinsic twist, $\Omega_{03} = 0$, and find a solution of system (11)–(14) that is

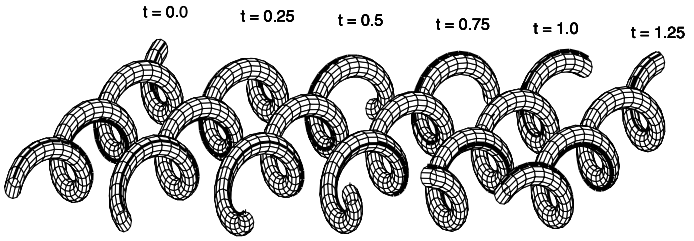

Fig. 3. Wave dynamics with bend and shear displacement for a helical rod.

independent of s so that the centerline of the rod is a straight line. This corresponds to $\vec{\gamma} = \vec{\Omega} = 0$, $\omega_1 = \omega_3 = \Gamma_2 = 0$ and nonzero variables $\omega_2(t)$, $\Gamma_1(t)$, $\Gamma_3(t)$. In this case the system (11)–(14) reduces to

$$\frac{\partial \omega_2}{\partial t} = -C_3 \Gamma_1 (\Gamma_3 - \Gamma_{03}) + \Gamma_1 \Gamma_3, \tag{28}$$

$$\frac{\partial \Gamma_1}{\partial t} + \omega_2 \Gamma_3 = 0, \tag{29}$$

$$\frac{\partial \Gamma_3}{\partial t} - \omega_2 \Gamma_1 = 0. \tag{30}$$

After integrating once we find the two identities

$$\Gamma_1^2 + \Gamma_3^2 = \Pi^2, \qquad \omega_2^2 + C_3(\Gamma_3 - \Gamma_{03})^2 + \Gamma_1^2 = 2E, \tag{31}$$

where Π and E are constants. Substitution of (31) into the reduced system (28)–(30) yields

$$\frac{\mathrm{d}\Gamma_3}{\sqrt{\left(\Pi^2 - \Gamma_3^2\right)\left(2E - \Pi^2 - C_3(\Gamma_3 - \Gamma_0)^2 + \Gamma_3^2\right)}} = \mathrm{d}t.$$

The last integration leads to elliptic functions.

The solution represents a simple physical motion in which all of the local frames rotate in the same direction simultaneously. The excitation has infinite phase velocity and zero group velocity, thus it is not a wave but an oscillation of the entire rod. A qualitative picture of the motion can be easily obtained in the small amplitude limit directly from the system (28)–(30). The approximate solution is

$$\omega_2 = A\cos(\Gamma_0 t) + B\sin(\Gamma_0 t), \qquad \Gamma_1 = -A\sin(\Gamma_0 t) + B\cos(\Gamma_0 t), \quad \Gamma_3 = \Gamma_0,$$

where A and B are small arbitrary constants.

To observe pure shear oscillation in a numerical simulation, we specify an initial state that is strongly sheared. The initial shape is such that $\vec{d}_3$ is aligned, not along the axis of the rod, but rather normal to it, and the initial conditions are chosen to be consistent with Eqs. (28)–(30). For the simulation in Fig. 4, a constant intrinsic twist was also included in the initial conditions. One can see that every cross-section of the rod possesses angular velocity but the rod never bends. Instead, as all the cross-sections rotate in unison, the angular momentum is converted completely into shear.

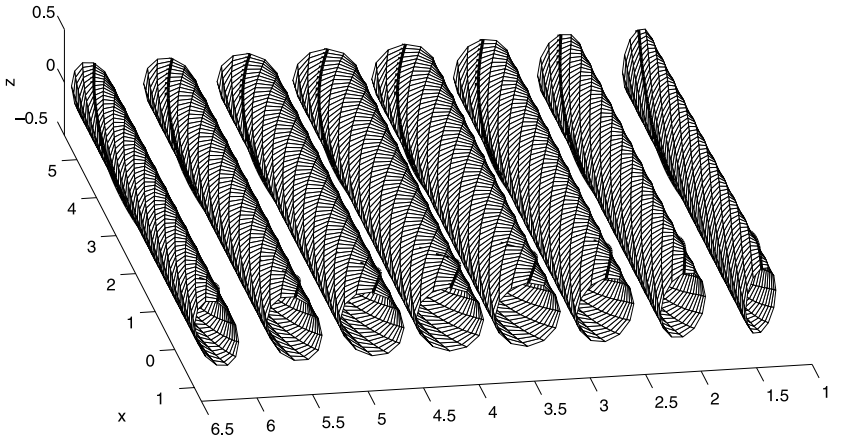

Fig. 4. Snapshots of pure shear oscillations of a twisted rod. The cross-sections remain circular for all times although the shear motion rotates them so that they appear to be deformed.

4. Bend and shear waves: approximate analytical solutions

4.1. Intrinsically straight, untwisted rod

In this section we consider rods that have an intrinsic shape defined by $\vec{\Omega}_0 = (0,0,0)$ and $\vec{\Gamma}_0 = (0,0,\Gamma_{03})$, where Γ_{03} is a constant. We then use a perturbation method to derive a planar approximate solution consisting of bend and shear.

The base (trivial) solution is given by all variables equal to zero except $\Gamma_3 = \Gamma_{03}$. For convenience we define the variable $\delta\Gamma_3 = \Gamma_3 - \Gamma_{03}$. If one tries to find a solution consisting of pure shear with no extension/compression (i.e. only γ_1 and Γ_1 nonzero), one finds that the only possibility is the straight rod translating at a constant speed. A similar situation arises if one attempts to find a pure bend solution (i.e. only ω_1 and Ω_1 nonzero). Thus bend and shear motions are required for even a simple solution.

The simplest motion of the rod that involves bend and shear has two polarizations: either γ_1, Γ_1, ω_2, and Ω_2 as nonzero variables or γ_2, Γ_2, ω_1, and Ω_1 as nonzero variables. It is also necessary to have nonzero values for γ_3 and $\delta\Gamma_3$, otherwise the system of equations reduces to wave equations for each variable and additional algebraic conditions that are generally inconsistent.

Since the bend and shear are restricted by the chosen polarization and since there is no twist in the rod, either $\vec{d}_1$ or $\vec{d}_2$ (depending on the polarization) will be constant and the solution describes a combined bend–shear motion in a plane that is orthogonal to the constant director.

We develop a perturbation scheme for each variable as follows:

$$G_k = \sum_{i=1} \epsilon^i G_k^{(i)} = \epsilon G_k^{(1)} + \epsilon^2 G_k^{(2)} + \cdots, \tag{32}$$

here $G_k^{(i)}$ designates the ith order term for the kth variable of the polarization γ_1, Γ_1, ω_2, Ω_2, γ_3, $\delta\Gamma_3$, and ϵ is a small parameter (perturbation amplitude). The first order terms $\gamma_3^{(1)}$ and $\delta\Gamma_3^{(1)}$ correspond to extension/compression (sound) waves that can propagate entirely independent of bend–shear in the linear approximation. Thus, we assume that $\gamma_3^{(1)} = \delta\Gamma_3^{(1)} = 0$ in the expansion (32).

Our perturbation scheme yields the linear system for the first order variables (with superscripts omitted):

$$\frac{\partial\gamma_1}{\partial t} = \frac{\partial\Gamma_1}{\partial s}, \tag{33}$$

$$\frac{\partial \omega_2}{\partial t} = D_1 \frac{\partial \Omega_2}{\partial s} + \Gamma_1 \Gamma_{03}, \tag{34}$$

$$\frac{\partial \Gamma_1}{\partial t} + \omega_2 \Gamma_{03} = \frac{\partial \gamma_1}{\partial s}, \tag{35}$$

$$\frac{\partial \Omega_2}{\partial t} = \frac{\partial \omega_2}{\partial s} \tag{36}$$

and for the second order variables $\gamma_3^{(2)}$ and $\delta\Gamma_3^{(2)}$ (superscripts omitted):

$$\frac{\partial \gamma_3}{\partial t} - \omega_2 \gamma_1 = C_3 \frac{\partial \delta\Gamma_3}{\partial s} - \Gamma_1 \Omega_2, \tag{37}$$

$$\frac{\partial \delta\Gamma_3}{\partial t} - \omega_2 \Gamma_1 = \frac{\partial \gamma_3}{\partial s} - \Omega_2 \gamma_1. \tag{38}$$

Under the given assumptions, the second order variables $\gamma_1^{(2)}$, $\Gamma_1^{(2)}$, $\omega_2^{(2)}$ and $\Omega_2^{(2)}$ yield four more equations that coincide with (33)–(36). So the second order solutions for $\gamma_1^{(2)}$, $\Gamma_1^{(2)}$, $\omega_2^{(2)}$ and $\Omega_2^{(2)}$ have the same form as the first order solutions. We point out that setting $\gamma_3 = 0$ and $\delta\Gamma_3 = 0$, leads to four differential equations (33)–(36) for the four remaining unknowns plus two additional algebraic constraints, Eqs. (37) and (38), resulting in an overdetermined system which in general is inconsistent. Therefore, bend–shear waves require small amplitude extension/compression waves. At the end of this section, we describe a limiting case in which these constraints are satisfied.

The solution of the linear system (33)–(36) can be found assuming that each variable is proportional to $\exp(-i\omega t + iks)$ where ω is a frequency and k is a wavenumber. A simple calculation yields the consistency condition $(\omega^2 - D_1 k^2)(\omega^2 - k^2) = \omega^2 \Gamma_{03}^2$. The frequencies are

$$\omega_\pm = \frac{1}{2}\left\{ \sqrt{k^2\left(\sqrt{D_1}+1\right)^2 + \Gamma_{03}^2} \pm \sqrt{k^2\left(\sqrt{D_1}-1\right)^2 + \Gamma_{03}^2} \right\}. \tag{39}$$

In this formula we take into account only one sign of the frequency because the opposite sign corresponds only to propagation in the opposite direction.

Up to second order in ϵ, the solution for bend–shear waves in an intrinsically straight untwisted rod is

$$\omega_2 = \epsilon(1+\epsilon)\sin(\omega t - ks), \tag{40}$$

$$\Omega_2 = -\frac{k}{\omega}\epsilon(1+\epsilon)\sin(\omega t - ks), \tag{41}$$

$$\gamma_1 = \frac{k}{\omega}\frac{\omega^2 - D_1 k^2}{\omega \Gamma_{03}}\epsilon(1+\epsilon)\cos(\omega t - ks), \tag{42}$$

$$\Gamma_1 = -\frac{\omega^2 - D_1 k^2}{\omega \Gamma_{03}}\epsilon(1+\epsilon)\cos(\omega t - ks), \tag{43}$$

$$\gamma_3 = \frac{kC_3}{4\omega}\frac{\Gamma_{03}\epsilon^2}{(\omega^2 - k^2 C_3^2)}\cos(2\omega t - 2ks), \tag{44}$$

$$\delta\Gamma_3 = -\frac{\Gamma_{03}\epsilon^2}{4(\omega^2 - k^2 C_3^2)}\cos(2\omega t - 2ks), \tag{45}$$

where ω is either ω_+ or ω_-. Notice that the wavelength of the extension/compression wave is half the wavelength of the shear or bend waves.

Below we show that the wave can be characterized as predominantly bend or predominantly shear depending on frequency (ω_+ or ω_-) and the wave number. Numerical simulation of the nonlinear system (11)–(14) and estimations based on (39)–(43) support this characterization.

In the short wavelength limit, $k \to \infty$, we obtain two branches: $\omega_+ \approx \sqrt{D_1}k$ and $\omega_- \approx k$, corresponding to the usual dispersion relations for bend and shear ($\omega \approx k\sqrt{D/I}$ and $\omega \approx k\sqrt{C/\rho}$, respectively, in dimensional variables).

In the long wavelength limit, $k \to 0$, we obtain $\omega_+ = \Gamma_{03}$ for shear waves and $\omega_- \approx k^2\sqrt{D_1}/\Gamma_{03}$ for bend waves. The last one corresponds to the well-known parabolic relation for flexural waves ($\omega = k^2 R\sqrt{Y/\rho_{\text{volume}}}/2\Gamma_{03}$ in dimensional variables) [2].

To characterize the wave motion, we use the asymptotic solutions in Eqs. (40)–(43) to estimate the ratio of shear to bend $|\Gamma_1|/|\Omega_2|$ for both branches (ω_+ and ω_-) as presented in Fig. 5. When this ratio is very small, we conclude that the dynamics consist of mostly bend and little shear. On the other hand, when this ratio is large, we conclude that the dynamics consist of mostly shear and little bend. Using (40)–(43) and the dispersion relation for large values of k, we find that $|\Gamma_1| \ll |\Omega_2|$ for ω_+ and $|\Gamma_1| \gg |\Omega_2|$ for ω_-. For small values of k these relations reverse direction, so that for moderate values of k there is a combination of shear and bend waves.

We also determine the maximum displacement of the rod centerline due to bend–shear deformations. It can be determined by integration of (1) and (2) and is equivalent to

$$\frac{k\Gamma_{03}\epsilon}{\omega_\pm(\omega_\pm^2 - k^2)}.$$

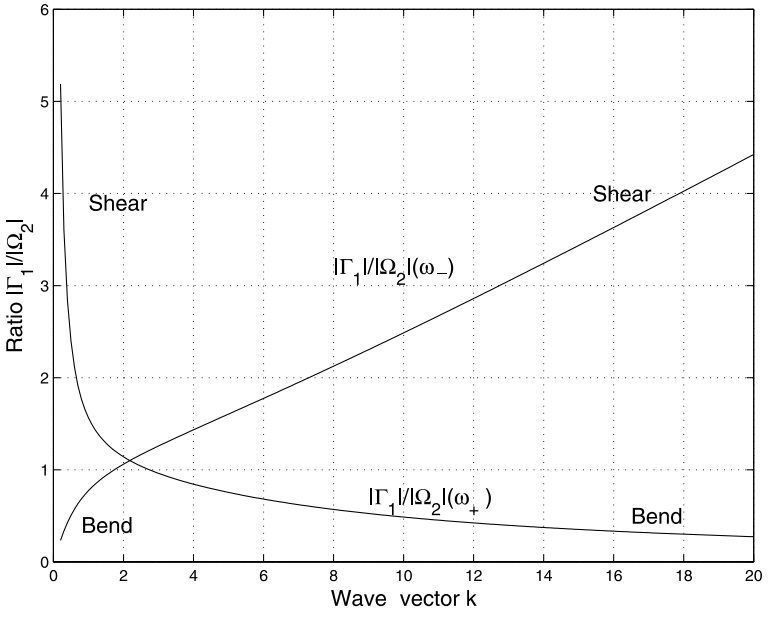

Fig. 5. Ratio of $|\Gamma_1|/|\Omega_2|$ versus wavenumber for different eigenvalues ω_+ and ω_-.

The analysis of this section shows that there are two separate bend–shear wave polarizations for an intrinsically untwisted rod. Each polarization corresponds to a planar motion of the rod. The waves in both cases are physically identical and posses the same wave velocity, dispersion and all other properties; the only difference is that they propagate in planes that are perpendicular to each other. However, for the intrinsically twisted rod discussed in Section 3.1, these polarizations cannot be excited separately. Instead the two polarization are combined with a phase shift of one-fourth of the twist period. This leads to the helix presented in that section.

A similar wave propagation phenomenon exists for the propagation of polarized light in birefringent crystals. In free space, light has two electromagnetic wave polarizations which are physically identical. But when the light propagates through an inhomogeneous medium, i.e. a birefringent crystal, the two polarizations become distinguishable as ordinary and extraordinary waves with different properties. Each wave is circularly polarized with the electric or magnetic vectors rotating in different directions. It is only because the medium is inhomogeneous that the waves propagate differently.

Finally, we mention that it is possible to obtain a shear wave with small bend deformation and no extension-compression. From (40)–(43) we find that if we set $\gamma_3 = 0$ and $\delta\Gamma_3 = 0$, the constraint in Eq. (37) is satisfied identically and the constraint in Eq. (38) is satisfied only when $\omega^2 - k^2 = 0$. Since $\omega_- \approx k$ as $k \to \infty$, the expressions for ω_2, Ω_2, γ_1, and Γ_1 in (40)–(43) are, up to second order in ϵ, the solution of the system with zero extension/compression. From Fig. 5, one can see that this limiting case corresponds to a predominantly shear wave.

5. Bend and shear waves: numerical simulations

5.1. Numerical implementation and testing

The system (11)–(14) is solved numerically with periodic boundary conditions using the method of lines. It is possible to use other types of boundary conditions such as free-end, but for the purposes of investigating relationships between bend, shear and extension/compression waves, we will restrict this analysis to periodic boundary conditions.

The spatial derivative of a function $f(s,t)$ at locations $s = kh$ for $k = 0, 1, \ldots, N$ is approximated using the finite-difference ratio

$$\frac{\partial f}{\partial s}(s,t) \approx \frac{1}{12h}[f(s-2h,t) - 8f(s-h,t) + 8f(s+h,t) - f(s+2h,t)]$$

resulting in a coupled system of ODEs in time. This system is solved by a 4th order Runge–Kutta method with time-step control (see [47, p. 711]).

Our program is written in C++. We verified that the program possesses appropriate accuracy as a function of space and time discretization (e.g. reducing time step by a factor of two increases accuracy by factor of 2^4). For further validation, two conserved quantities are monitored during all simulations. Throughout the simulation, the energy (see Appendix A) does not vary from its initial value by more than 10^{-13}. The magnitude of each director differs from unity by less than 10^{-13}.

In addition to the above accuracy test, we conducted numerous physically motivated tests to validate the proper behavior. For an elastic rod with a given intrinsic shape $\vec{\Gamma}_0$, $\vec{\Omega}_0$ we obtain a static solution when all initial velocities are zero and the initial shape coincides with the intrinsic one. Such tests were conducted for rods that are intrinsically straight, circular and helical in conformation. We also obtained uniform longitudinal and transverse translations of each of these conformations of the rod for appropriately chosen initial velocities.

For a rod that is bent into a ring, we conducted two additional test cases: (1) rotation in the plane of the ring and (2) twist about the axis of the rod. For the first test, only a uniform longitudinal velocity, $\vec{\gamma} = (0, 0, \gamma_3)$, was assigned. In this case, the ring begins to rotate and expand. As it expands, the rotational velocity decreases up to the point when the centrifugal force causing the expansion is balanced by the elastic extension of the rod. Then the ring begins to contract and the rotational velocity increases. The system continues to oscillate in this manner.

As a separate test of case (1), we set up initial conditions such that the centrifugal force and extension of the rod were balanced. In this case the radius remains constant and the ring rotates with constant velocity. For the rotation of an intrinsically straight rod bent into a ring, i.e. $\vec{\Omega}_0 = (0, 0, 0)$ and $\vec{\Gamma}_0 = (0, 0, 1)$, the only nonzero variables in the system (11)–(14) are γ_3, ω_1, Γ_3, and Ω_1 (variables γ_3, ω_2, Γ_3, and Ω_2 can be used instead). A simple calculation leads to the force balance $\gamma_3^2/\Gamma_3 = C_3(\Gamma_3 - \Gamma_{03})$. Here, the left side is proportional to the centrifugal force and the right side proportional to the extension force in the rod. Since the radius of the ring is $R = 1/\Omega_1$, and its circumference is $L\Gamma_3$, where L is the fiducial arclength, we can determine Ω_1 and ω_1.

For case (2) we analyzed two types of uniform twist motion for a rod that is bent into a closed circle. The behavior of each type depends on the intrinsic shape. If the circular rod has no intrinsic bend or twist, then the corresponding solution is a rotation around the longitudinal axis with constant angular velocity ($\omega_3 = \text{const}$). Such solution was found by Tobias et al. [48] for the Kirchhoff rod. If the circular rod is intrinsically circular ($\Omega_{02} = \text{const}$) then the solution is a rotation around the longitudinal axis with periodically changing angular velocity ω_3. In any case both types of uniform twist can be found from the reduced system:

$$\begin{aligned} \frac{\partial \omega_3}{\partial t} &= -D_1 \Omega_{02} \Omega_1, \\ \frac{\partial \Omega_1}{\partial t} &= \omega_3 \Omega_2, \\ \frac{\partial \Omega_2}{\partial t} &= -\omega_3 \Omega_1. \end{aligned} \tag{46}$$

If there is no intrinsic bend (i.e. $\Omega_{02} = 0$) then $\omega_3 = \text{const}$ and the ring rotates about its centerline with uniform angular velocity expressed by $\Omega_1 = A \sin \omega_3 t$, $\Omega_2 = A \cos \omega_3 t$. For the circular rod which has intrinsic bend (i.e. $\Omega_{02} = \text{const} \neq 0$) the solutions are elliptic functions.

5.2. Simulation of an untwisted rod

In this section we perform numerical simulations of the solution of the nonlinear system of Eqs. (11)–(14) for the case of the intrinsically straight, untwisted rod. We used as initial conditions the approximate solutions derived in Section 4.1, Eqs. (40)–(45), and periodic boundary conditions.

To quantify the agreement between the nonlinear numerical solutions and our approximate analytic solutions the energy in the rod as a function of time is evaluated both numerically and analytically using the approximate solutions. The total energy is obtained from the integral

$$E = \frac{1}{2} \int_0^L \left\{ |\vec{\gamma}|^2 + \vec{\omega} \cdot (\hat{I}\vec{\omega}) + (\vec{\Gamma} - \vec{\Gamma}_0) \cdot (\hat{C}(\vec{\Gamma} - \vec{\Gamma}_0)) + (\vec{\Omega} - \vec{\Omega}_0) \cdot (\hat{D}(\vec{\Omega} - \vec{\Omega}_0)) \right\} \mathrm{d}s$$

(see Appendix A for more details).

The characterization of a bend–shear wave as predominantly bend or shear can also be quantified by computing the dot product $\vec{d}_3 \cdot \vec{\Gamma}/|\vec{\Gamma}| = \Gamma_3/|\vec{\Gamma}|$, since $\vec{\Gamma}$ is tangent to the rod centerline and $\vec{d}_3$ is perpendicular to the cross-sections. When this dot product is near 1 then $\vec{\Gamma} \approx \Gamma_3 \vec{d}_3$, and there is very little shear.

However, bend, twist and extension/compression may be large. The type of wave, predominantly bend or predominantly shear, is observed to be determined by the choice of sign in (39) in agreement with the analysis based on the approximate solutions.

Snapshots from a simulation using the full nonlinear system of equations, with the choice of ω_+ and parameter values $k = 2$, $\epsilon = 0.5$ and $\Gamma_{03} = 1$, are presented in Fig. 6. The five snapshots correspond to the times $t = 0.0$, $t = 0.9$, $t = 1.8$, $t = 2.7$ and $t = 3.6$ from top to bottom and show the change in the shape of the rod over one period of oscillation in time. Adjacent cross-sections are not parallel as they would be if the motion is predominantly shear.

Since the numerical simulation is based on the solution of the nonlinear system of equations, the value of ϵ is completely arbitrary. In the asymptotic solution obtained in Section 4.1, ϵ is the small parameter and should therefore be chosen accordingly. The value used here, $\epsilon = 0.5$, is somewhat large in order to visualize the solution more easily. We point out that although the approximate solutions shown in Eqs. (42)–(45), which are used as initial conditions for the numerical simulation, contain only simple trigonometric functions, the integration of Eqs. (1) and (2) results in expressions involving the composition of trigonometric functions. This leads to the complex behavior shown in Fig. 6.

Each component of the total energy is computed during the nonlinear simulations and compared to the corresponding value obtained by integrating the first-order approximate solutions (40)–(45). For the simulation presented in Fig. 6, the numerical and approximate values differed by less than 1% over the duration of the simulation.

Fig. 7 shows $\Gamma_3/|\vec{\Gamma}|$ as a function of s at a fixed time for large wave number $k = 8$ and two different initial conditions: one with ω_- and one with ω_+ in (40)–(45). The value of ϵ was chosen for each set of initial conditions so as to yield the same total energy. The dotted line in Fig. 7 corresponds to the choice $\omega = \omega_-$ and is consistent with a predominantly shear displacement. The choice of initial conditions based on $\omega = \omega_+$, the solid line in Fig. 7, produces very little shear; in fact, the elastic energy due to bend in this simulation is about seven times larger than the elastic energy due to shear. For small wave number ($k < 1$) a similar picture is obtained (data not shown) but ω_- corresponds to the small oscillations of $\Gamma_3/|\vec{\Gamma}|$ and ω_+ to the large oscillations, consistent with the analytic results presented in Fig. 5.

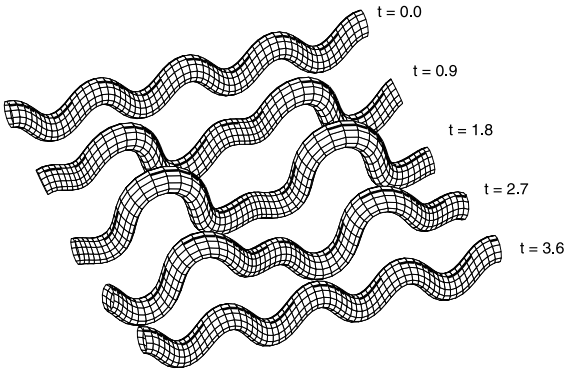

Fig. 6. Bend–shear wave with predominantly bend displacement. Five snapshots from a simulation with predominantly bend displacement represent one period of oscillation of the rod in time. The initial perturbation amplitude, ϵ, is 0.5. The bold thick lines on the top of the tubes indicate that the rod is untwisted. Cross-sections indicate that the motion is predominantly bend not shear ($\Omega_2 > \Gamma_1 > 0$).

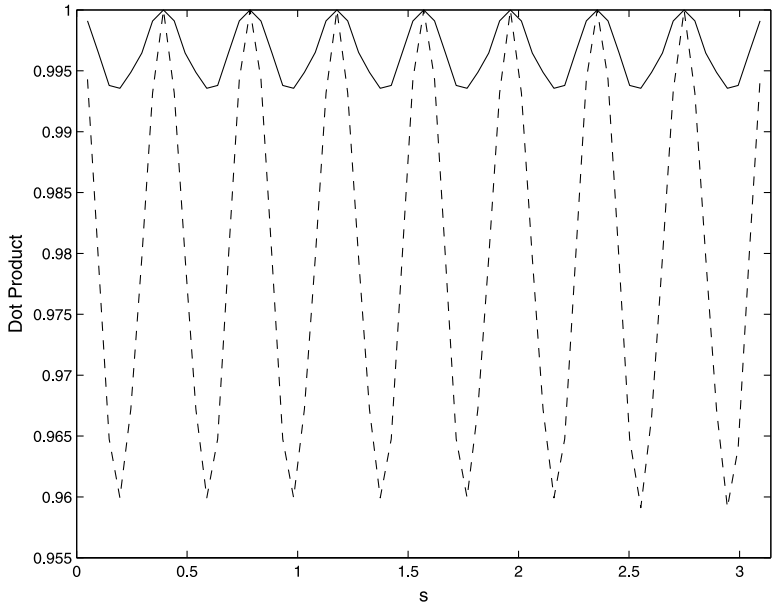

Fig. 7. Dot product for bend and shear waves versus fiducial arclength. Dotted line corresponds to ω_- and solid line corresponds to ω_+.

6. Application: dynamics of DNA

There has been much interest recently in using various elastic rod models to describe the structure of DNA. Here we make a direct comparison between dynamics of elastic rod as determined by Eqs. (11)–(14) and results obtained from an all atom molecular dynamics simulation of DNA. Since molecular dynamics simulations utilize an atom based energy function that represents chemical bonds, van der Waals and electrostatic interactions and no explicit inclusion of elastic energy terms, then there is no a prior requirement that the two models produce similar results. Our goal is to determine if such an atomic based physicochemical description of DNA supports elastic rod type motions.

For this purpose we have constructed a three dimensional all-atom model of 158 base-pairs of DNA, corresponding to approximately one persistence length of DNA. For this length of DNA we expect the elastic rod approximation to be valid. Full details of both simulations are presented below.

6.1. Elastic rod simulation

While the physical dimensions and intrinsic shape of DNA and nucleosomes [28] have been determined at atomic resolution by X-ray crystallography, the elastic properties of DNA are not so well defined despite numerous efforts. Experimental determination of the elastic constants of DNA includes the traditional measurement of the speed of sound through bulk DNA [29,30] as well as single molecule techniques utilizing scanning tunneling microscopy [31], fluorescence microscopy [32], fluorescence correlation spectroscopy [33], optical tweezers [34,35], magnetic beads [36,37], optical micro-fibers [38], low energy electron point sources (electron holography) [39] and atomic force microscopy (AFM) [40]. Since each method differs in the molecular properties being probed, the spatial and temporal resolution achieved, the molecular environment, and sample preparation techniques, each method yields similar but not exactly the same value for the elastic constants. The constants used here are as described in Section 2.1.

The intrinsic shape is that of a straight rod with constant twist density, Ω_{03}, and length $L\Gamma_{03}$, thus $\vec{\Gamma}_0 = (0, 0, \Gamma_{03})$ and $\vec{\Omega}_0 = (0, 0, \Omega_{03})$, corresponding to idealized B from DNA. We orient the rod in the laboratory frame along the Y-axis and choose to orient the internal frame at $s = 0$ such that $\vec{d}_1$ is parallel to the Z-axis and $\vec{d}_2$ is parallel to the X-axis (these choices are arbitrary). The initial deformation of the rod centerline is a sinusoidal displacement of amplitude A along the Z-axis given by $\vec{r}(s, 0) = (0, \Gamma_{03}s, A\cos(2\pi s/L))$. We further specify that this displacement be entirely due to shear, i.e. there is no initial bend or extension/compression in the rod. This implies that the initial bend is $\vec{\Omega}(s, 0) = \vec{\Omega}_0$. It also means that $\vec{d}_3$ is initially constant and given by $\vec{d}_3 = (0, 1, 0)$. The other two directors, $\vec{d}_1$ and $\vec{d}_2$ rotate in the XZ-plane to accommodate the twist. The initial condition for the shear is then given by

$$\vec{\Gamma}(s, 0) = \hat{T}^{-1}\frac{\mathrm{d}\vec{r}}{\mathrm{d}s}(s, 0),$$

where $\hat{T}$ is the transformation matrix from the internal frame to the laboratory frame. In this case

$$\hat{T}^{-1} = \begin{pmatrix} \sin(\Omega_{03}s) & 0 & \cos(\Omega_{03}s) \\ \cos(\Omega_{03}s) & 0 & -\sin(\Omega_{03}s) \\ 0 & 1 & 0 \end{pmatrix}. \tag{47}$$

We also assign an initial velocity which in the laboratory frame has the form $\vec{v}(s, 0) = (0, 0, A_v \sin(2\pi s/L))$, i.e. the initial velocity is purely translational, with amplitude corresponding to 1 Å/ps. These initial conditions produce a motion of the elastic rod that remains planar for all time. Table 1 provides the exact functional forms of the initial conditions used in the elastic rod simulation.

6.2. All-atom simulation

For the molecular dynamics simulations the compute engine NAMD [50] was used to integrate Newton's equations of motion. The bonded, van der Waals and electrostatic energy functions are as described in the CHARMM22 all-atom force field for nucleic acids [51]. The simulation of DNA was thus a typical molecular dynamics simulation of DNA with the following two exceptions. First, periodic boundary conditions were enforced only along the long axis of the DNA and the ends of each strand of the DNA were not free but rather chemically bond to one another, i.e. the 5′ and 3′ ends of each strand were ligated. Thus, the DNA was topologically equivalent to a circle, so it was necessary to have an integer number of helical turns of the DNA. The unit cell was chosen so that the periodic boundaries passed through these two bonds at $t = 0$, but no such restriction was imposed by NAMD. Periodicity of the physical dimensions and chemical structure of the DNA was required so that the all-atom and elastic rod simulations would have the same boundary conditions. Periodicity of the chemical structure had the added benefit of removing end effects, such as unwinding of the DNA helix, that occurs in molecular dynamic simulations with the usual free end boundary conditions.

Second, no water or counterions were included in the simulation and an electrostatics cut-off at 10 Å was used. Thus the DNA could not dissipate energy to the environment, and long range electrostatic interac-

Table 1
Initial conditions for planar bend–shear simulations

Function	Initial value (internal frame)
$\vec{\gamma}$	$(A_v \cdot \sin(2\pi s/L) \cdot \cos(\Omega_{03}s), -A_v \cdot \sin(2\pi s/L) \cdot \sin(\Omega_{03}s), 0)$
$\vec{\omega}$	$(0, 0, 0)$
$\vec{\Gamma}$	$(A \cdot \sin(2\pi s/L) \cdot \cos(\Omega_{03}s), -A \cdot \sin(2\pi s/L) \cdot \sin(\Omega_{03}s), \Gamma_{03})$
$\vec{\Omega}$	$(0, 0, \Omega_{03})$

tions were not included in the all-atom simulations. Our focus is on whether the atomic structure of DNA supports elastic rod type motions so for comparison with the elastic rod model, which is a Hamiltonian system, it is important to remove interaction with the environment in the all-atom simulation. In regards to electrostatics, it has been demonstrated that simulations of DNA in the gas phase with no modification of the long range electrostatic interactions do not yield biologically observed structures of DNA on the time scale of 100's of nanoseconds [52]. However, [52] also demonstrates that on the sub-nanosecond timescale, as investigated here, that the structure of DNA in the gas phase is largely stable.

Since all energy terms and corresponding parameters are determined by the CHARMM22 force field we were only free to specify initial conditions in the molecular dynamics simulation. In order to compare the elastic rod and all-atom models, the same internal coordinate functions used to specify the elastic rod initial conditions were also used to initiate the molecular dynamics simulation. Note that the elastic rod simulation uses dimensionless variables while the model of DNA must be specified in dimensional variables.

To convert the internal coordinate description in Table 1 to an all-atom representation of DNA, a random sequence of 158 base-pairs of DNA was generated and the internal coordinates were assumed to have a one-to-one correspondence to the DNA helical parameters [27] as follows: $\Omega = (\text{roll}, \text{tilt}, \text{twist})$ and $\Gamma = (\text{shift}, \text{slide}, \text{rise})$. With this assumption Ω and Γ were converted to an all-atom model of DNA using the DNA analysis software 3DNA [49]. To obtain initial velocities for the molecular dynamics simulation consistent with the elastic rod model, random initial velocities representing a temperature of 300 K were first assigned, as is typical in molecular dynamics simulations and then the desired sinusoidal velocity along the length of the rod, as listed in Table 1 was added to the thermal velocities. Thus the molecular dynamics simulation included thermal motion which is not defined in the elastic rod model. Note that even with zero thermal motion the initial conditions specified in Table 1 may produce a motion in the DNA that becomes nonplanar.

Fig. 8 presents snapshots of the dynamics of an intrinsically twisted rod while Fig. 9 presents the dynamics of 158 base-pairs of DNA from the molecular dynamics simulation. Remarkably, in the all-atom model the initial sinusoidal disturbance is observed to propagate along the structure with a constant velocity. For the elastic rod model, the wave speed was estimated from the numerical results to be 1.4 Å/ps using the scalings in Eq. (15) and are based on the rod's mechanical properties. For the molecular dynamics simulation, the wave speed was estimated to be 2.2 Å/ps based on graphical observations. This is a result of the choice of force field which has no elastic energy term. This molecular dynamics simulation was run for a total of 600 ps and no significant deviations from planarity or dissipation of the wave into thermal motion was observed.

A total of three molecular dynamics simulations with different initial velocities, $A_v = 0, 1$, and 5 Å/ps, were conducted. In the simulation with zero initial velocity the DNA began to oscillate, indicating that the

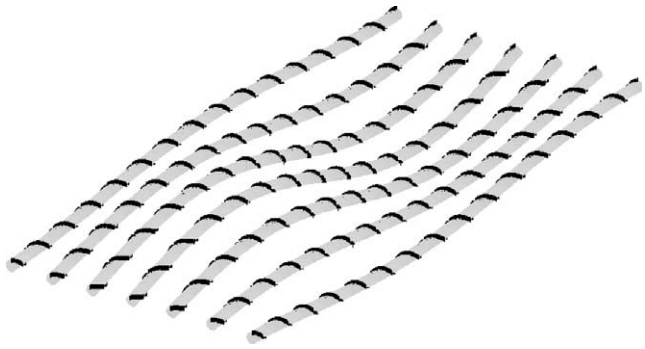

Fig. 8. Planar bend wave dynamics from the elastic rod model. The dark solid line indicates twist.

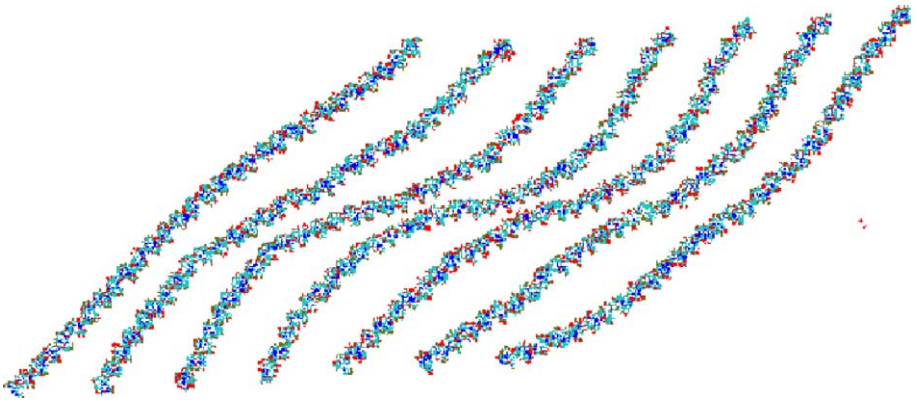

Fig. 9. Planar dynamics of 158 base-pairs of DNA from the Molecular Dynamics simulation.

intrinsic shape of the 158 base-pairs of DNA tends to be a straight twisted rod, even though the intrinsic shape is defined only as a sum of molecular mechanics potential terms. In the simulation with initial velocity amplitude of 5.0 Å/ps, the DNA developed nonplanar motions and rather severe distortions from ideal base stacking. The distortions from ideal base stacking can be expected when DNA is assigned such a large momentum. The deviations from planarity are an indication that the chemical linkage in DNA produces coupling between modes that are not captured by our simple elastic rod model in which the matrices $\hat{C}$ and $\hat{D}$ are diagonal and not base-pair specific.

7. Conclusion

We have analyzed the propagation of bend and shear deformations in a geometrically exact elastic rod model. Our analysis applies to any long thin fiber that can be treated as a homogeneous rod, e.g. biopolymers such as DNA and filamentous proteins. We have investigated the large amplitude dynamics of intrinsically twisted and untwisted rods and have found numerical and analytical solutions that contain bend/shear waves. In some cases, we have been able to provide exact solutions of the nonlinear system of equations and in other cases we have developed asymptotic solutions based on perturbations of known steady states. The solutions and the numerical simulations focused on the role of shear and bend waves and on the amount of extension/compression required in the solutions. The main reason for this is that previous investigations often include the assumptions of rod inextensibility and zero shear, leading to a lesser understanding of the role of these excitations.

It was shown that each of the two branches of the dispersion relation corresponding to the intrinsically untwisted rod can be treated as bend or shear wave only in the limits $k \to 0$ or $k \to \infty$. But in general the rod dynamics include a combination of shear and bend waves. For the intrinsically twisted rod, each branch mentioned above splits into two branches. The behavior of these four branches can be determined as bend (shear) only in the limit $k \to \infty$. In the long wavelength limit $k \to 0$, they have a combination of bend and shear displacement. When $k \to \Omega_{03}$, one of the branches in Fig. 2 indicates pure shear and a second brach indicates pure bend.

We have compared the results from an all-atom molecular dynamics simulation of 158 base-pairs of DNA to those obtained from the elastic rod model. Although the two models are completely different, the results are in very good agreement. The molecular dynamics simulation demonstrates that, in the absence of a surrounding medium, the chemical structure of DNA supports elastic wave propagation and that the

gross properties of DNA, on the scale of one persistence length, dominate over known inhomogeneities at the scale of base-pairs. In order for the continuum model to be more directly applicable to DNA simulations, the elastic rod model must be modified to include the interaction of the rod with an environment to which energy can dissipate. In addition, further analysis of the molecular dynamics simulations will enable identification of the contribution that each component of the molecular mechanics force field makes to the elastic properties of DNA.

Acknowledgements

This work was conducted in the Center for Computational Science at Tulane and Xavier Universities and in the Theoretical Molecular Biology Laboratory which was established under NSF Cooperative Agreement Number OSR-9550481/LEQSF (1996–1998)-SI-JFAP-04 and supported by the Office of Naval Research (NO-0014-99-1-0763). R. Cortez's work was partly funded by NSF grant #DMS-0094179 and by DOE grant #DE-FG02-01ER63119. O.O. Zhmudsky's work was supported by DOE grant #DE-FG02-01ER63119.

Appendix A. Conservation law for the general case

Let us take the dot product of Eq. (3) with $\vec{\gamma}$ and Eq. (4) on the $\vec{\omega}$. Also we multiply Eq. (5) on the left by the matrix $\hat{C}$ and then take the dot product with $\vec{\Gamma} - \vec{\Gamma}_0$. We multiply Eq. (6) on the left by the matrix $\hat{D}$ and then take the dot product with $\vec{\Omega} - \vec{\Omega}_0$. The equations become

$$\rho\vec{\gamma}\cdot\frac{\partial\vec{\gamma}}{\partial t} = \vec{\gamma}\cdot\frac{\partial\hat{C}(\vec{\Gamma}-\vec{\Gamma}_0(s))}{\partial s} + \vec{\gamma}\cdot\left(\vec{\Omega}\times\left(\hat{C}\left(\vec{\Gamma}-\vec{\Gamma}_0\right)\right)\right), \tag{A.1}$$

$$\vec{\omega}\cdot\frac{\partial\hat{I}\vec{\omega}}{\partial t} = \vec{\omega}\cdot\frac{\partial\hat{D}(\vec{\Omega}-\vec{\Omega}_0(s))}{\partial s} + \vec{\omega}\cdot\left(\vec{\Omega}\times\left(\hat{D}\left(\vec{\Omega}-\vec{\Omega}_0\right)\right)\right) + \vec{\omega}\cdot\left(\vec{\Gamma}\times\left(\hat{C}\left(\vec{\Gamma}-\vec{\Gamma}_0\right)\right)\right), \tag{A.2}$$

$$\begin{aligned}&(\vec{\Gamma}-\vec{\Gamma}_0(s))\cdot\frac{\partial\hat{C}(\vec{\Gamma}-\vec{\Gamma}_0(s))}{\partial t} + (\vec{\Gamma}-\vec{\Gamma}_0(s))\cdot\left(\hat{C}\left(\vec{\omega}\times\vec{\Gamma}\right)\right)\\ &\quad= (\vec{\Gamma}-\vec{\Gamma}_0(s))\cdot\frac{\partial\hat{C}\vec{\gamma}}{\partial s} + (\vec{\Gamma}-\vec{\Gamma}_0(s))\cdot\left(\hat{C}\left(\vec{\Omega}\times\vec{\gamma}\right)\right),\end{aligned} \tag{A.3}$$

$$(\vec{\Omega}-\vec{\Omega}_0(s))\cdot\frac{\partial\hat{D}\vec{\Omega}}{\partial t} + (\vec{\Omega}-\vec{\Omega}_0(s))\cdot\left(\hat{D}\left(\vec{\omega}\times\vec{\Omega}\right)\right) = (\vec{\Omega}-\vec{\Omega}_0(s))\cdot\frac{\partial\hat{D}\vec{\omega}}{\partial s}. \tag{A.4}$$

This yields:

$$\begin{aligned}&\frac{1}{2}\frac{\partial}{\partial t}\left\{\rho|\vec{\gamma}|^2 + \vec{\omega}\cdot(\hat{I}\vec{\omega}) + (\vec{\Gamma}-\vec{\Gamma}_0)\cdot(\hat{C}(\vec{\Gamma}-\vec{\Gamma}_0)) + (\vec{\Omega}-\vec{\Omega}_0)\cdot(\hat{D}(\vec{\Omega}-\vec{\Omega}_0))\right\}\\ &\quad= \frac{\partial}{\partial s}\left\{\vec{\gamma}\cdot(\hat{C}(\vec{\Gamma}-\vec{\Gamma}_0)) + \vec{\omega}\cdot(\hat{D}(\vec{\Omega}-\vec{\Omega}_0))\right\} + \vec{\gamma}\cdot(\vec{\Omega}\times(\hat{C}(\vec{\Gamma}-\vec{\Gamma}_0)))\\ &\qquad+ (\vec{\Gamma}-\vec{\Gamma}_0)\cdot\hat{C}(\vec{\Omega}\times\vec{\gamma}) + \vec{\omega}\cdot(\vec{\Omega}\times(\hat{D}(\vec{\Omega}-\vec{\Omega}_0))) - (\vec{\Omega}-\vec{\Omega}_0)\cdot\hat{D}(\vec{\omega}\times\vec{\Omega})\\ &\qquad+ \vec{\omega}\cdot(\vec{\Gamma}\times(\hat{C}(\vec{\Gamma}-\vec{\Gamma}_0))) - (\vec{\Gamma}-\vec{\Gamma}_0)\cdot\hat{C}(\vec{\omega}\times\vec{\Gamma}).\end{aligned} \tag{A.5}$$

It is easy to show that the sum of the last six term is equal to zero. For example, with the use of vector identities, the third and the fourth terms can be written as

$$(\hat{C}(\vec{\Gamma}-\vec{\Gamma}_0))(\vec{\gamma}\times\vec{\Omega})+(\vec{\Gamma}-\vec{\Gamma}_0)\hat{C}(\vec{\Omega}\times\vec{\gamma}), \tag{A.6}$$

which is zero since $\hat{C}$ is diagonal. The same applies to other terms in the equation, leaving only the conservation law

$$\frac{\partial\mathscr{E}}{\partial t}=\frac{\partial\mathscr{P}}{\partial s}, \tag{A.7}$$

where the following definitions are used:

$$\begin{aligned}\mathscr{E}&=\frac{1}{2}\left\{\rho|\vec{\gamma}|^2+\vec{\omega}\cdot(\hat{I}\vec{\omega})+(\vec{\Gamma}-\vec{\Gamma}_0)\cdot(\hat{C}(\vec{\Gamma}-\vec{\Gamma}_0))+(\vec{\Omega}-\vec{\Omega}_0)\cdot(\hat{D}(\vec{\Omega}-\vec{\Omega}_0))\right\},\\ \mathscr{P}&=\left\{\vec{\gamma}\cdot(\hat{C}(\vec{\Gamma}-\vec{\Gamma}_0))+\vec{\omega}\cdot(\hat{D}(\vec{\Omega}-\vec{\Omega}_0))\right\}.\end{aligned} \tag{A.8}$$

Here, $\mathscr{E}$ corresponds to the energy density (kinetic and potential) in the rod at any time t and location s, and $\mathscr{P}$ corresponds to the momentum density (linear and angular) in the rod at any time t and location s.

Integrating Eq. (A.7) in space yields

$$\frac{\mathrm{d}E}{\mathrm{d}t}\equiv\frac{\mathrm{d}}{\mathrm{d}t}\int_0^L\mathscr{E}(s,t)\mathrm{d}s=\mathscr{P}(L,t)-\mathscr{P}(0,t),$$

which equals zero for periodic boundary conditions used here. Therefore we obtain the associated integral of the motion

$$E=\frac{1}{2}\int_0^L\left\{|\vec{\gamma}|^2+\vec{\omega}\cdot(\hat{I}\vec{\omega})+(\vec{\Gamma}-\vec{\Gamma}_0)\cdot(\hat{C}(\vec{\Gamma}-\vec{\Gamma}_0))+(\vec{\Omega}-\vec{\Omega}_0)\cdot(\hat{D}(\vec{\Omega}-\vec{\Omega}_0))\right\}\mathrm{d}s.$$

References

[1] J.C. Simo, J.E. Marsden, P.S. Krishnaprasad, The hamiltonian structure of nonlinear elasticity: the material and convective representations of solids, rods and plates, Arch. Rational Mech. Anal. 104 (1988) 125–183.
[2] A.E.H. Love, A Treatise on the Mathematical Theory of Elasticity, Dover Publications, New York, 1944.
[3] E.H. Dill, Kirchhoff's theory of rods, Arch. History Exact Sci. 44 (1) (1992) 1–23.
[4] J. Coyne, Analysis of the formation and elimination of loops in twisted cable, IEE J. Oceanic Eng. 15 (1990) 72–83.
[5] E.E. Zajac, Stability of two planar loop elasticas, Trans. ASME 29 (1962) 136–142.
[6] Y. Sun, J.W. Leonard, Dynamics of ocean cables with local low-tension regions, Ocean Eng. 25 (1998) 443–463.
[7] M.A. Vaz, M.H. Patel, Three dimensional behaviour of elastic marine cables in sheared currents, Appl. Ocean Res. 22 (1) (2000) 45–53.
[8] A. Goriely, M. Tabor, Spontaneous helix-hand reversal and tendril perversion in climbing plants, Phys. Rev. Lett. 80 (1998) 1564–1568.
[9] A. Goriely, T. McMillen, The shape of a cracking whip, Phys. Rev. Lett. 88 (2002) 244.
[10] C.J. Benham, An elastic model of the large structure of duplex DNA, Biopolymers 18 (1979) 609–623.
[11] M.L. Bret, Relationship between the energy of superhelix formation, the shear modulus, and the torsional brownian motion of DNA, Biopolymers 17 (8) (1978) 1939–1965.
[12] T. Schlick, Modeling superhelical DNA: recent analutical and dynamic approaches, Curr. Opin. Struct. Biol. 5 (1995) 245–262.
[13] O. Gonzalez, J.H. Maddocks, Extracting parameters for base-pair level models of DNA from molecular dynamics simulations, Theoret. Chem. Accounts 106 (1–2) (2001) 76–82.
[14] Y. Shi, J.E. Hearst, The kirchhoff elastic rod, the nonlinear schrodinger equation, and DNA supercoiling, J. Chem. Phys. 101 (6) (1994) 5186–5200.

[15] Y. Shi, A.E. Borovik, J.E. Hearst, Elastic rod model incorporating shear extension, generalized nonlinear schrödinger equations, and novel closed-form solutions for super coiled DNA, J. Chem. Phys. 103 (1995) 3166.
[16] J.E. Hearst, Y. Shi, New solutions for the stationary states of the elastic rod model are useful in the representation of DNA configuration in the living cell, Nonlinear Sci. Today 5 (1) (1995) 1–49.
[17] T.C. Bishop, J.E. Hearst, Potential function describing the folding of the 30 nm fiber, J. Phys. Chem. B 102 (1998) 6433–6439.
[18] T. Bishop, O. Zhmudsky, Information transmission along DNA, Curr. Computat. Mol. Biol. 2001 (2001) 105–106.
[19] M. Nizzete, A. Goriely, Towards a classification of Euler–Kirchhoff filaments, J. Math. Phys. 40 (1999) 2830–2866.
[20] A. Goriely, M. Tabor, Nonlinear dynamics of filaments. I. Dynamical instabilities, Physica D 105 (20) (1997) 45–61.
[21] B.D. Coleman, E. Dill, D. Swigon, On the dynamics of flexure and stretch in the theory of elastic rods, Arch. Rational Mech. Anal. 129 (1995) 147.
[22] S.S. Antman, T. Liu, Traveling waves in hyperelastic rods, Quart. Appl. Math. 36 (1979) 377.
[23] D. Dichmann, J. Maddocks, R. Pego, Hamiltonian dynamics of an elastica and the stability of solitary waves, Arch. Rational Mech. Anal. 135 (1996) 357.
[24] L. Landau, E. Lifshitz, Fluid Mechanics, Pergamon Press, Oxford, 1959.
[25] L. Landau, E. Lifshitz, Electrodynamics of Continuous Media, Pergamon Press, Oxford, 1960.
[26] M. McClain, Y. Shi, T. Bishop, J.E. Hearst, Visualization of exact hamiltonian dynamics solutions, unpublished.
[27] R. Dickerson, Definitions and nomenclature of nucleic acid structure component, Nucl. Acids Res. 17 (5) (1989) 1797–1803.
[28] K. Luger, A. Maeder, R. Richmond, D. Sargent, T. Richmond, Crystal structure of the nucleosome core particle at 2.8 a resolution, Nature 389 (1997) 251–260.
[29] G. Maret, R. Oldenbourg, F. Winterling, K. Dransfeld, A. Rupprecht, Velocity of high frequency sound waves in oriented DNA fibers and films determined by brillouin scattering, Colloid Polym. Sci. 257 (10) (1979) 1017–1020.
[30] M.B. Hakim, S.M. Lindsay, J. Powell, The speed of sound in DNA, Biopolymers 23 (1984) 1185.
[31] R. Guckenberger, M. Heim, C. Cevc, H. Knapp, W. Wiegräbe, A. Hillebrand, Scanning tunneling microcopy of insulators and biological speciments based on lateral conductivity of ultrathin water films, Science 266 (1994) 1538–1540.
[32] M. Yanagida, Y. Hiraoka, I. Katsura, Dynamic behaviors of DNA molecules in solution studied by fluorescence microscopy, Cold Spring Harbor Symp. Quant. Biol. 47 (1983) 177–187.
[33] S. Wennmalm, L. Edman, R. Rigler, Conformational fluctuations in single DNA molecules, Proc. Natl. Acad. Sci. 94 (20) (1997) 10641–10646.
[34] S. Smith, Y. Cui, C. Bustamante, Overstretching B-DNA: the elastic response of individual double-stranded and single-strandede DNA molecules, Science 271 (1996) 759.
[35] D. Wang, H. Yin, R. Landick, J. Gelles, S. Block, Stretching DNA with optical tweezers, Biophys. J. 72 (1997) 1335.
[36] S. Smith, L. Finzi, C. Bustamante, Direct mechanical measurements of the elasticity of single DNA molecules by using magnetics beads, Science. 258 (1992) 1122.
[37] T.R. Strick, J.F. Allemand, D. Bensimon, A. Bensimon, V. Croquette, The elasticity of a single supercoiled DNA moleculae, Science 271 (1996) 1835.
[38] P.A. Lebrun, C. Heller, R. Lavery, J. Viovy, D. Chatenay, F. Caron, DNA: an extensible molecule, Science 271 (1996) 792–794.
[39] H.W. Fink, C. Schonenberger, Electrical conduction through DNA molecules, Nature 398 (1999) 407–410.
[40] H.G. Hansma, R. Sinsheimer, M. Li, P. Hansma, Atomic force microscopy of single- and double-stranded DNA, Nucl. Acids Res. 20 (1992) 3585–3590.
[41] L. Landau, E. Lifshitz, Theory of Elasticity, Pergamon Press, Oxford, 1986.
[42] D.S. Horowitz, J.C. Wang, Torsional rigidity of DNA and length dependence of the free energy of DNA supercoiling, J. Mol. Biol. 173 (1984) 75.
[43] P.J. Heath, J.B. Clendenning, B.S. Fujimoto, J.M. Schurr, Effect of bending strain on the torsion elastic constant of DNA, J. Mol. Biol. 260 (1996) 718.
[44] C. Bouchiat, M. Mezard, Elasticity model of a super coiled DNA molecule, Phys. Rev. Lett. 80 (7) (1998) 1556.
[45] J.D. Moroz, P. Nelson, Entropic elasticity of twist-storing polymers, Macromolecules 31 (1998) 6333.
[46] T.P. Westcott, I. Tobias, W.K. Olson, Modeling self-contact forces in the elastic theory of DNA supercoilling, J. Chem. Phys. 107 (10) (1997) 3967–3980.
[47] W.H. Press, S.A. Teukolsky, W.T. Vetterling, B.P. Flannery, Numerical Recipes in Fortran 77, Cambridge University Press, Cambridge, 1992.
[48] I. Tobias, B.D. Coleman, M. Lembo, A class of exact dynamical solutions in the elastic rod model of DNA with implications for the theory of fluctuations in the torsional motion of plasmids, J. Chem. Phys. 105 (6) (1996) 2517–2526.
[49] Xiang-Jun Lu, Wilma K. Olson, 3DNA: a software package for the analysis, rebuilding and visualization of three-dimensional nucleic acid structures, Nucl. Acids Res. 31 (17) (2003) 5108–5121.

[50] L. Kale, R. Skeel, M. Bhandarkar, R. Brunner, A. Gursoy, N. Krawetz, J. Phillips, A. Shinozaki, K. Varadarajan, K. Schulten, Namd2: Greater scalability for parallel molecular dynamics, J. Comp. Phys. 151 (1999) 283–312.
[51] A.D. MacKerell, N. Banavali, All-atom empirical force field for nucleic acids: 2) application to molecular dynamics simulations of DNA and RNA in solution, J. Comp. Chem. 21 (2000) 105–120.
[52] M. Reuda, S.G. Kalko, F.J. Lugue, M. Orozco, The structure and dynamics of DNA in the gas phase, J. Am. Chem. Soc. 125 (26) (2003) 8007–8014.